Available online at www.sciencedirect.com
SCIENCE DIRECT
Journal of Photochemistry and Photobiology A: Chemistry 176 (2005) 78–85
Journal of Photochemistry and Photobiology A:Chemistry
www.elsevier.com/locate/jphotochem

Photodissociation dynamics of CH_3CFCl_2 and $CDCl_3$ at 205–209 nm

Michio Mashino, Hidetaka Yamada, Akihiro Sugita, Masahiro Kawasaki *

Department of Molecular Engineering and Graduate School of Global Environmental Studies, Kyoto University, Kyoto 615-8510, Japan

Available online 19 October 2005

Abstract

Photodissociation dynamics of CH_3CFCl_2 (HCFC-141b) and $CDCl_3$ at 205–209 nm have been studied by the photofragment velocity map imaging technique. The velocity distributions and the anisotropy parameters of hydrogen atom and chlorine atom consist of fast and slow components. From these results, the photoexcitation of CH_3CFCl_2 at 205–209 nm is inferred to proceed via a mixture of the $A' \leftarrow A'$ and $A'' \leftarrow A'$ transitions for direct cleavage of the C–Cl bond, while via the $A' \leftarrow A'$ transition for direct cleavage of the C–H bond. The photodissociation of $CDCl_3$ proceeds mainly via the $E \leftarrow A_1$ transition for the formation of Cl. The direct C–D bond cleavage process is a minor channel and is attributable to the $A_1 \leftarrow A_1$ transition. The photodissociation dynamics of CF_2Cl_2 and $CFCl_3$ has also been investigated.

Keywords: HCFC-141b; Chloroform; CF_2Cl_2; $CFCl_3$; Electronic transition

1. Introduction

The photochemistry of halocarbons has been placed in the focus of attention since their ozone depletion potential in the stratosphere was recognized [1,2]. Continuing efforts have been made to clarify the mechanism of photochemical reactions in the atmosphere [3–5]. The studies on photodissociation processes have also yielded benefits towards molecular dynamics. Among hydrochlorofluorocarbons, CH_3CFCl_2 (HCFC-141b) is utilized as a replacement for $CFCl_3$ in the manufacturing process of closed-cell insulating foams and for $CFCl_2CF_2Cl$ in a variety of industrial processes. On the basis of the heat of reaction for CH_3CFCl_2, the following photodissociation processes are plausible at around 200 nm for production of H and Cl photofragments [6]:

$$CH_3CFCl_2 \rightarrow CH_2CFCl_2 + H, \quad \Delta H^\circ = 107\,\text{kcal mol}^{-1} \tag{1}$$

$$CH_3CFCl_2 \rightarrow CH_3CFCl + Cl/Cl^*, \quad \Delta H^\circ = 82/84\,\text{kcal mol}^{-1} \tag{2a/2b}$$

$$CH_3CFCl_2 \rightarrow CH_2CFCl + Cl/Cl^* + H, \quad \Delta H^\circ = 123/125\,\text{kcal mol}^{-1} \tag{3a/3b}$$

The product yields from the photodissociation of CH_3CFCl_2 at 193 nm were reported under cold molecular beam conditions: 0.15 for H and 0.85 for total of $Cl(^2P_{3/2})$ and $Cl^*(^2P_{1/2}$, 2.5 kcal mol^{-1} above the ground state) [7]. At room temperature, the total quantum yield for Cl and Cl^* becomes unity due to different Franck–Condon factors [6]. In the vibrationally mediated photodissociation, the angular anisotropy parameters for Cl and Cl^* from the vibrationally hot parent molecules in $\nu_{CH} = 3$ or 4 at 235 nm are reported to be small positive values due to the vibration-enhanced mixing of different electronic states upon excitation [8].

Similarly, the photodissociation dynamics of simpler chlorinated molecules, $CHCl_3$, CF_2Cl_2 and $CFCl_3$, was studied by several groups [9–17]. On the basis of the heat of reaction for $CHCl_3$, CF_2Cl_2 and $CFCl_3$, the following processes are plausible at around 200 nm [11,15]:

$$CHCl_3 \rightarrow CCl_3 + H, \quad \Delta H^\circ = 95\,\text{kcal mol}^{-1} \tag{4}$$

$$CHCl_3 \rightarrow CHCl_2 + Cl/Cl^*, \quad \Delta H^\circ = 76/78\,\text{kcal mol}^{-1} \tag{5a/5b}$$

$$CF_2Cl_2 \rightarrow CF_2Cl + Cl/Cl^*, \quad \Delta H^\circ = 83/85\,\text{kcal mol}^{-1} \tag{6a/6b}$$

$$CFCl_3 \rightarrow CFCl_2 + Cl/Cl^*, \quad \Delta H^\circ = 74/76\,\text{kcal mol}^{-1} \tag{7a/7b}$$

* Corresponding author. Tel.: +81 75 383 2572; fax: +81 75 383 2573.
E-mail address: kawasaki@moleng.kyoto-u.ac.jp (M. Kawasaki).

1010-6030/$ – see front matter © 2005 Elsevier B.V. All rights reserved.
doi:10.1016/j.jphotochem.2005.09.006

The dissociation of $CHCl_3$ at 193 nm under cold molecular beam conditions was reported by Yang et al. [11] and under collision-free conditions at room temperature by Brownsword et al. [13]. The direct C–H bond rupture from an electronically excited state was not observed. In the latter experiments, H atom formation was attributed to a two-photon process in which the secondary photolysis of the $CHCl_2$ radicals follows the primary photolysis processes (5a) and (5b).

In this work, we have reported the photodissociation dynamics of CH_3CFCl_2, $CDCl_3$, CF_2Cl_2 and $CFCl_3$ at 205–209 nm, measuring the translational energy and angular distributions of the atomic photofragments with the velocity map imaging spectroscopic technique.

2. Experimental

A Nd^{3+}:YAG pumped dye laser (5 ns, 10 Hz) was used. Dye laser frequencies tripled to 205.09 and 205.14 nm were used in the one-color pump-and-probe scheme to dissociate molecules under supersonic molecualr beam condtions, and to ionize D or H photofragments, respectively, by (2 + 1) resonance-enhanced multiphoton ionization (REMPI) via the two-photon transitions 3^2S, $3^2D \leftarrow 1^2S$. The 205 nm laser light (~0.2 mJ/pulse) was generated by the mixing of the two laser beams at 615 and 308 nm in a BBO crystal. Similarly, frequencies tripled to 207.06 or 208.96 nm were used to dissociate molecules, and to ionize the Cl or Cl^* atomic fragments by a (2 + 1) REMPI scheme via $5^2P_{1/2} \leftarrow {}^2P_{3/2}$, and $5^2P_{1/2} \leftarrow {}^2P_{1/2}$, respectively. The laser light was focused with a lens (f = 0.20 m) on the pulsed molecular beam of each compound. The position of the lens was adjusted for the frequency tripled light (3ω) to avoid unexpected interference by the frequency doubled light (2ω), although these laser lights were simultaneously introduced into the interaction region. The photofragments by 2ω would be easily distinguishable from that by 3ω in ion images, because the electric vectors of 2ω and 3ω lights were perpendicular to each other. It should be noted that there was no photofragment by 2ω under our conditions. The samples were diluted ~10% in Ar with the backing pressure of 750 Torr. The temperature in the molecular beam was estimated to be about 10 K from the rotational temperature of NO under similar conditions.

The atomic ions, H^+, D^+ and Cl^+, were detected by the velocity map imaging technique [18]. Briefly, the ions were focused onto a microchannel plate (MCP) mounted on the end of a flight tube. Electrons ejected from the MCP hit a phosphor screen. The image on the screen was recorded by a CCD camera and accumulated in a personal computer. The observed image was back-projected to reconstruct the three-dimensional (3D) velocity distribution by a method similar to that used in computerized tomography [19,20]. Then, the slice image of 3D velocity distribution was extracted to obtain an angular anisotropy parameter, β, by a least-squares fit of the slice to the angular distribution function:

$$I(\theta) = \left(\frac{1}{4\pi}\right)(1 + \beta P_2(\cos\theta)), \tag{8}$$

where $I(\theta)$ is the normalized angular distribution of the photofragment and θ is the angle between the polarization vector of the photolysis laser radiation and the fragment recoil velocity vector. $P_2(\cos\theta)$ is the second-order Legendre polynomial. For the prompt dissociation, the anisotropy parameter can be written as

$$\beta = 2P_2(\cos\ \chi) = 3\ \cos^2\ \chi - 1, \tag{9}$$

where χ is the angle between the dissociation direction and the transition dipole direction [21–23].

3. Results

3.1. Formation of hydrogen atom and deuterium atom at 205 nm

3.1.1. CH_3CFCl_2

The photofragment image of hydrogen atoms shown in Fig. 1a is the equatorial slice through the 3D velocity distribution. The angular distribution is attributable mainly to the perpendicular optical transition. The center-of-mass translational energy distribution, $P(E_T)$, and the anisotropy parameter, $\beta(E_T)$ are shown in Fig. 2a and b, respectively. $P(E_T)$ becomes zero at 32 kcal mol^{-1}, which corresponds to the maximum available kinetic energy released to a H atom by one-photon in reaction (1). As shown in Fig. 2a, $P(E_T)$ can be fitted with two different components:

$$P(E_T) = aP_G(E_T) + bP_B(E_T), \tag{10}$$

where a and b are coefficients, and $(a + b)$ is unity. The higher energy component is represented by a Gaussian energy distribution, $P_G(E_T)$, with an average energy $\langle E_T\rangle$ = 13 kcal mol^{-1} and a standard deviation σ = 7 kcal mol^{-1}. The energy width is 14 kcal mol^{-1}. The lower energy distribution is represented by a Maxwell–Boltzmann energy distribution, $P_B(E_T)$, with translational temperature $T = (4.8 \pm 0.4) \times 10^3$ K. The mixing ratio of 0.6 ± 0.1 for the Gaussian distribution, a, is obtained by a best-fit method. These results are summarized in Table 1.

The distribution of $\beta(E_T)$ shown in Fig. 2b consists of two different components. With use of the anisotropy parameters for the Gaussian and Maxwell–Boltzmann energy distributions, β_G and β_B, the experimentally observed $\beta(E_T)$ is fitted to the following equation:

$$\beta(E_T) = \frac{a\beta_G P_G(E_T) + b\beta_B P_B(E_T)}{aP_G(E_T) + bP_B(E_T)} \tag{11}$$

The coefficients are taken as a = 0.6 and b = 0.4 from the fitting parameters for the translational energy distribution. For a Maxwell–Boltzmann energy distribution, an isotropic angular distribution is expected due to the indirect dissociation process with a long lifetime of the parent molecule: $\beta_B = 0$. By best-fitting $\beta(E_T)$ to Eq. (11), we obtained $\beta_G = -0.6 \pm 0.2$ (Table 2).

3.1.2. $CDCl_3$

Fig. 3a shows the 3D slice of the D photofragment image from the photodissociation of $CDCl_3$, which gives $P(E_T)$ and $\beta(E_T)$ in

Table 1
Best-fit parameters for Maxwell–Boltzmann and Gaussian distributions for the hydrogen or deuterium photofragments at 205 nm

Parent molecule	Maxwell–Boltzmann $P_B(E_T)$	Gaussian $P_G(E_T)$		Population of Gaussian component, a
	T ($\times 10^3$ K)	$\langle E_T \rangle$ (kcal mol^{-1})	σ (kcal mol^{-1})	
CH_3CFCl_2	4.8 ± 0.4	13	7	0.6 ± 0.1
$CDCl_3$	5.0 ± 0.4	30	7	0.1 ± 0.1

σ is a standard deviation in a Gaussian energy distribution.

Table 2
Angular anisotropy parameters for the Gaussian energy distributions, β_G, in the one-photon photodissociation at 205–209 nm

Parent molecule	H or D	$Cl(^2P_{3/2})$	$Cl^*(^2P_{1/2})$
CH_3CFCl_2	-0.6 ± 0.2	0.6 ± 0.1	0.9 ± 0.1
$CDCl_3$	2.2 ± 0.3	0.7 ± 0.2	–
CF_2Cl_2	–	1.1 ± 0.1	1.4 ± 0.1
$CFCl_3$	–	0.3 ± 0.1	0.3 ± 0.1

Fig. 4a and b. By the best-fit method, $P(E_T)$ is resolved into two parts: $P_G(E_T)$ with $\langle E_T \rangle = 30$ and $\sigma = 7$ kcal mol^{-1}, and $P_B(E_T)$ with $T = (5.0 \pm 0.4) \times 10^3$ K. The mixing ratio for the Gaussian distribution is 0.1 ± 0.1 (Table 1), indicating that the direct C–D bond rupture is a minor process in the D atom formation. As shown in Fig. 4b, $\beta(E_T)$ increases from 0 to 1 with E_T. β_G for the fast D atom is obtained to be 2.2 ± 0.3 with use of $a = 0.1$ and $\beta_B = 0$.

3.2. Formation of chlorine atoms at 207 and 209 nm

3.2.1. CH_3CFCl_2

Photofragment images of Cl and Cl* from CH_3CFCl_2 are shown in Fig. 1b and c, respectively. The corresponding $P(E_T)$s are shown in Fig. 5a and c. The maximum observed translational energies correspond to the maximum available energies, 52 and 48 kcal mol^{-1}, released in the one-photon dissociation via reactions (2a) and (2b), respectively. As shown in Fig. 5a, $P(E_T)$ for Cl is decomposed into the Gaussian and Maxwell–Boltzmann energy distributions. The mixing ratio for the Gaussian distribution, a, is calculated to be 0.7 ± 0.1. The same mixing ratio for Cl* is obtained in Fig. 5c. These fitting parameters are listed in Table 3. Fig. 5b and d show $\beta(E_T)$ for Cl and Cl* between $E_T = 20$ and 40 kcal mol^{-1}, which is best-fitted to Eq. (11) with $a = 0.7$ and $\beta_B = 0$. We obtained $\beta_G = 0.6 \pm 0.1$ for Cl and $\beta_G = 0.9 \pm 0.1$ for Cl* (Table 2).

3.2.2. $CDCl_3$

The photofragment image of Cl from $CDCl_3$ is shown in Fig. 3b. The maximum possible translational energy released in the one-photon dissociation via reactions (5a) and (5b) is 62 kcal mol^{-1}. As seen in Fig. 6a, the distribution exceeds this maximum energy, indicating that some Cl fragments are produced from a two-photon process. Thus, $P(E_T)$ up to $E_T = 62$ kcal mol^{-1} is fitted with two components. The best-fit values, $\langle E_T \rangle = 32$ kcal mol^{-1}, $\sigma = 10$ kcal mol^{-1}, $T = (7.0 \pm 0.6) \times 10^3$ K, and $a = 0.4 \pm 0.1$ are obtained (Table 3). Although the contribution of the two-photon process is appreciable, we will focus our discussion on the one-photon dissociation processes. For Cl in Fig. 6b, $\beta(E_T)$ between 20–40 kcal mol^{-1} consists of two different components: $\beta_G = 0.7 \pm 0.2$ and $\beta_B = 0$.

3.2.3. CF_2Cl_2 and $CFCl_3$

Fig. 7 shows $P(E_T)$s for Cl and Cl* from CF_2Cl_2 and $CFCl_3$. Those $P(E_T)$s are best-fit with two different components: $P_G(E_T)$ and $P_B(E_T)$, neglecting contributions of the two-photon processes that appear only at the higher energy region. The anisotropy parameters and fitting parameters are summarized in Tables 2 and 3, respectively.

4. Discussion

4.1. Photodissociation of CH_3CFCl_2 at 205–209 nm

4.1.1. Formation of Cl and Cl* atoms

The A band of CH_3CFCl_2 is broad in the UV region and assigned to the ($\sigma^* \leftarrow$ n) transition localized on the C–Cl bonds.

Table 3
Best-fit parameters for the Maxwell–Boltzmann and Gaussian distributions of chlorine photofragments at 207–209 nm

Parent molecule	Photoflagment atom	Maxwell–Boltzmann $P_B(E_T)$	Gaussian $P_G(E_T)$		Population of Gaussian component, a
		T ($\times 10^3$ K)	$\langle E_T \rangle$ (kcal mol^{-1})	σ (kcal mol^{-1})	
CH_3CFCl_2	$Cl(^2P_{3/2})$	7.0 ± 0.3	30	7	0.7 ± 0.1
	$Cl^*(^2P_{1/2})$	8.1 ± 0.2	30	7	0.7 ± 0.1
$CDCl_3$	Cl	7.0 ± 0.6	32	10	0.4 ± 0.1
	Cl*	–	–	–	–
CF_2Cl_2	Cl	7.1 ± 0.6	30	7	0.8 ± 0.1 (0.7)
	Cl*	7.8 ± 0.6	30	7	0.7 ± 0.1 (0.7)
$CFCl_3$	Cl	8.1 ± 0.2	35	7	0.4 ± 0.1 (0.5)
	Cl*	9.4 ± 0.3	35	7	0.5 ± 0.1 (0.6)

σ is a standard deviation in a Gaussian energy distribution. Numbers in parentheses are the results of the 187 nm photodissociation in Ref. [15].

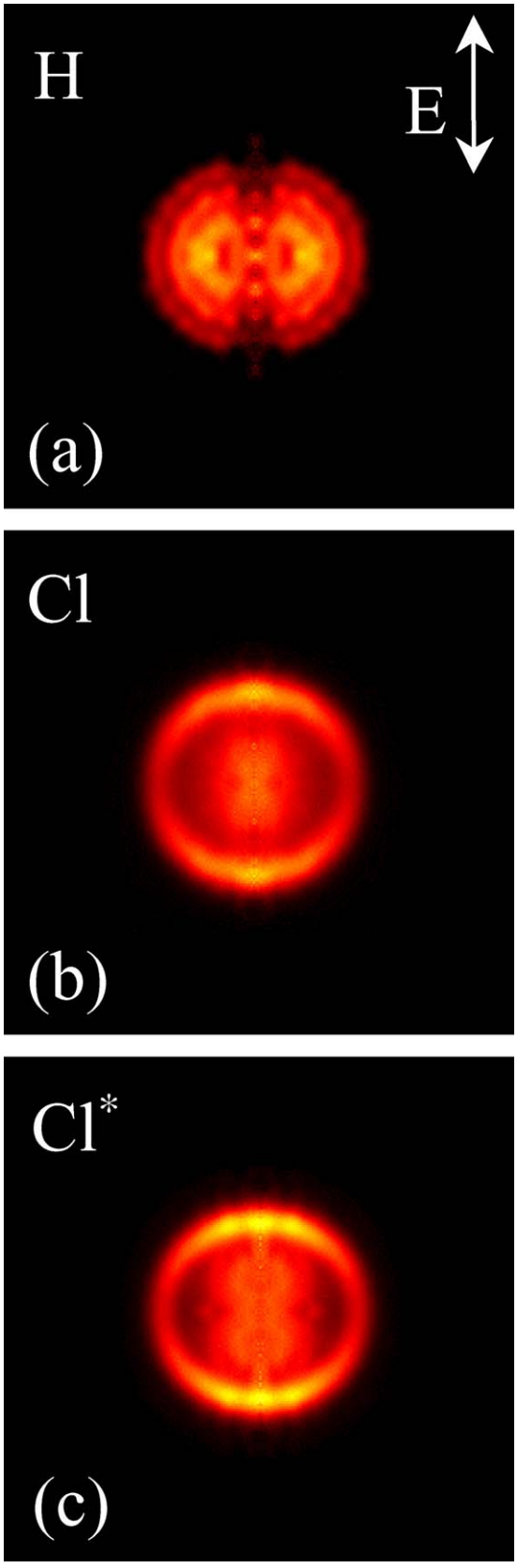

Fig. 1. Photofragment images of H, Cl and Cl^* atoms from CH_3CFCl_2 at 205, 207 and 209 nm, respectively, are displayed as equatorial slices through the reconstructed three-dimensional distributions. The arrow shows the direction of the electric vector of the photolysis laser.

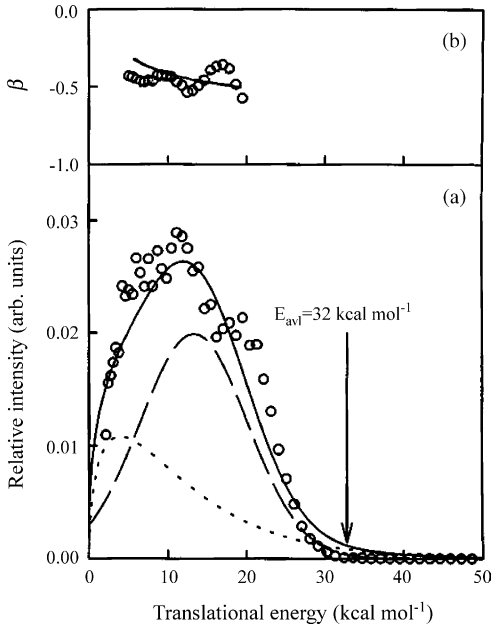

Fig. 2. H atom formation from CH_3CFCl_2 at 205 nm. (a) Center-of-mass translational energy distribution, $P(E_T)$. E_{avl} is the maximum available energy in the one-photon process for reaction (1). The broken and dotted curves are the best-fitted Gaussian and Maxwell–Boltzmann distributions, respectively. See Table 1 for fitting parameters. The solid curve is a sum of the two distributions. (b) Angular anisotropy parameters. The solid curve is the best-fit distribution obtained by Eq. (11) with population of the Gaussian energy distribution, $a = 0.6$.

[7,24]. The electronic transition dipole, μ, is in-plane (A′, μ_X or μ_Y) or out-of-plane (A″, μ_Z) in C_S symmetry with respect to the C–C–F molecular plane. μ_X has an angle of 56° with respect to the C–Cl bond and μ_Z has an angle of 34° assuming that (a) the transition is located on the Cl–C–Cl moiety which retains the structure of the ground state of CH_3CFCl_2 molecule, (b) μ_X is along the C_2 axis of the Cl–C–Cl, and (c) μ_Y is perpendicular to μ_X. The out-of-plane μ_Z is along the direction between two Cl atoms and perpendicular to the C_2 axis. The maximum β_Z value is calculated to be 1.06 for a A″ ← A′ transition, assuming the Cl–C–Cl angle = 112° [8,11]. The experimentally observed β values of Cl and Cl^* from the direct cleavage processes are 0.6 ± 0.1 and 0.9 ± 0.1, respectively (Table 2). The present positive low β values may be attributable to the mixing of a A″ ← A′ transition ($\beta_Z = 1.06$) with a A′ ← A′ transition ($\beta_X = -0.06$ or $\beta_Y = -1$).

According to Lauter et al. [6], the A″ state correlates with Cl at a large distance, while the A′ state correlates with Cl^*. However, the present β values for Cl and Cl^* are nearly the same. These results indicate that (a) the two different states couple to each other largely at the curve crossing and (b) the internal quenching from Cl^* to Cl occurs. Einfeld et al. [8] found that β values are 0.20 for Cl and 0.25 for Cl^* from the 235 nm photodissociation of CH_3CFCl_2 pre-excited to three and four quanta of C–H methyl stretches. They explained their results by the crossing between the two surfaces, which might be affected by the initial vibration excitation of the alkyl group. Similar effects are reported experimentally and theoretically for CX_3Y molecules [25–29]. The present β values (0.6–0.9) sug-

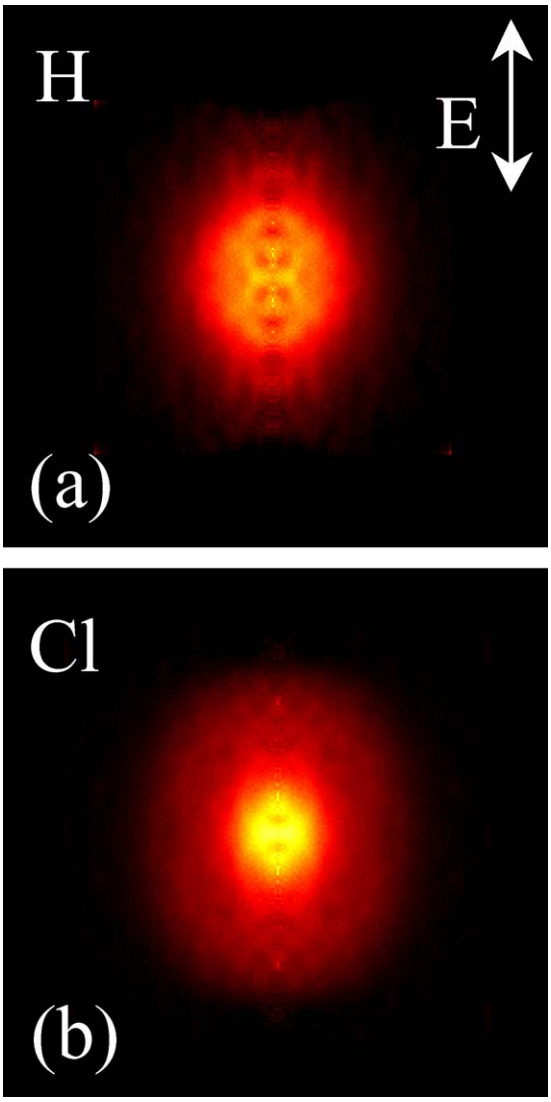

Fig. 3. Photofragment images of D and Cl atoms from $CDCl_3$ at 205 and 207 nm, respectively, are displayed as equatorial slices through the reconstructed three-dimensional distributions. The arrow shows the direction of the electric vector of the photolysis laser.

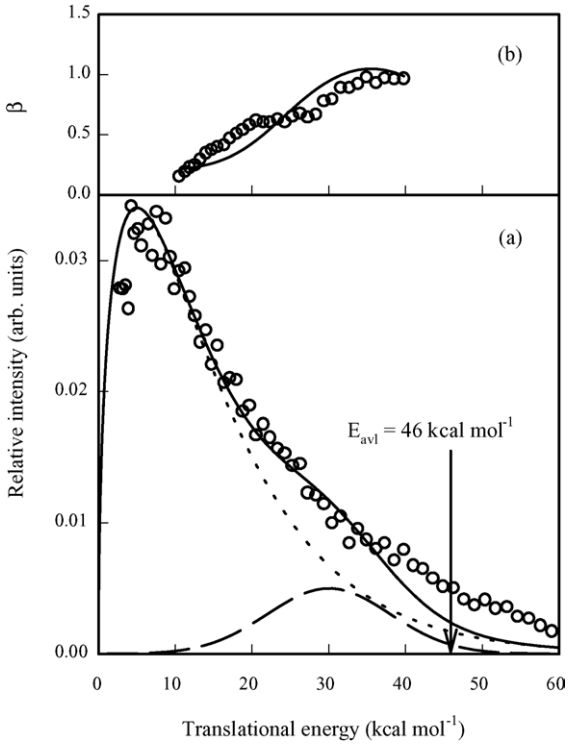

Fig. 4. D atom formation from $CDCl_3$ at 205 nm. (a) Center-of-mass translational energy distribution, $P(E_T)$. E_{avl} is the maximum available energy in the one-photon process for reaction (4). The broken and dotted curves are the best-fitted Gaussian and Maxwell–Boltzmann distributions, respectively. See Table 1 for the fitting parameters. The solid curve is the sum of two distributions. (b) Angular anisotropy parameters. The solid curve is the best-fit distribution obtained by Eq. (11) with $a = 0.1$.

gest that the mixing of the potential surfaces at the curve crossing is affected through vibration modes in the electronic excited states.

4.1.2. Formation of hydrogen atom

There are a direct (prompt dissociation) and an indirect (slow dissociation) C–H bond rupture processes, corresponding to the Gaussian and Maxwell–Boltzmann energy distributions, respectively. Based on the fact that the mixing ratio for the Gaussian distribution is 0.6 ± 0.1 and the previously reported quantum yield of the H formation is 0.15 at 193 nm [7], the quantum yields of the direct and indirect processes are estimated to be 0.09 ± 0.01 and 0.06 ± 0.01, respectively. Lauter et al. reported the quantum yield of the slow H atom at 193 nm is 0.04 [6]. Based on their interpretation, the indirect process for the H atom formation is attributed to a sequential mechanism: reactions (2a) and (2b) followed by the secondary formation of a H atom:

$$CH_3CFCl \rightarrow CH_2CFCl + H \quad (12)$$

As described above, the A band of CH_3CFCl_2 is assigned to a mixture of the $A' \leftarrow A'$ and $A'' \leftarrow A'$ transitions. The direct C-H bond rupture is characterized by a negative β value (-0.6). For the *XY* plane-polarized and the *Z* axis-polarized transitions, it is useful to use the addition theorem for $l = 2$ Legendre polynomials and average over the azimuthal angle in the C–C–F plane for the CH_3 group. This gives:

$$\text{for } \mu_X \quad \langle P_2(\cos\chi)\rangle = P_2\left(\cos\left(\frac{\varphi}{2}\right)\right) P_2(\cos\psi) \quad (13)$$

$$\text{for } \mu_Y \quad \langle P_2(\cos\chi)\rangle = P_2\left(\cos\left(\frac{\pi-\varphi}{2}\right)\right) P_2(\cos\psi) \quad (14)$$

$$\text{for } \mu_Z \quad \langle P_2(\cos\chi)\rangle = P_2\left(\cos\left(\frac{\pi}{2}\right)\right) P_2(\cos\psi) \quad (15)$$

where φ is the angle of C–C–F and ψ is that of C–C–H. If φ and ψ are equal to the tetrahedral angle, then, the β values for the *X*, *Y* and *Z* polarization are 0, $-1/3$ and 1/3, respectively [30]. The present results ($\beta = -0.6 \pm 0.2$) indicate that the $A' \leftarrow A'$ transition is μ_Y polarized in the C–C–F molecular plane. As described above, the $A' \leftarrow A'$ transition responsible to the direct formation of Cl and Cl^* could be polarized along μ_Y.

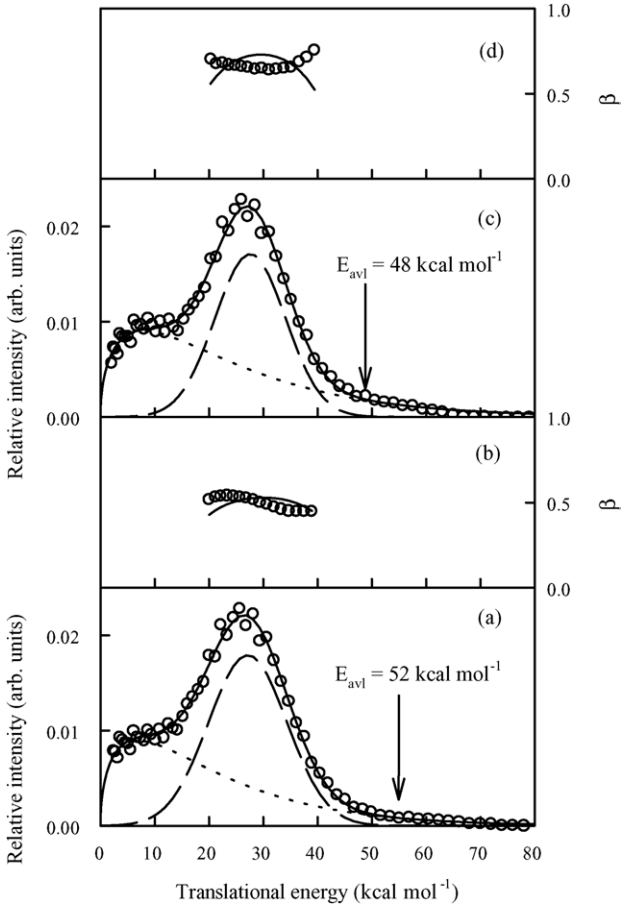

Fig. 5. Center-of-mass translational energy distributions, $P(E_T)$, for (a) Cl, (c) Cl^*, and angular anisotropy parameter for (b) Cl, (d) Cl^* from CH_3CFCl_2 at 207 nm (Cl) and 209 nm (Cl^*). E_{avl} is the maximum available energy for reaction (2). In (a) and (c), the dashed and dotted curves are the best-fitted Gaussian and Maxwell–Boltzmann distributions, respectively. See Table 3 for the fitting parameters. The solid curve is a sum of the two distributions. The solid curves in (b) and (d) are the best-fit distributions obtained by Eq. (11) with $a = 0.7$.

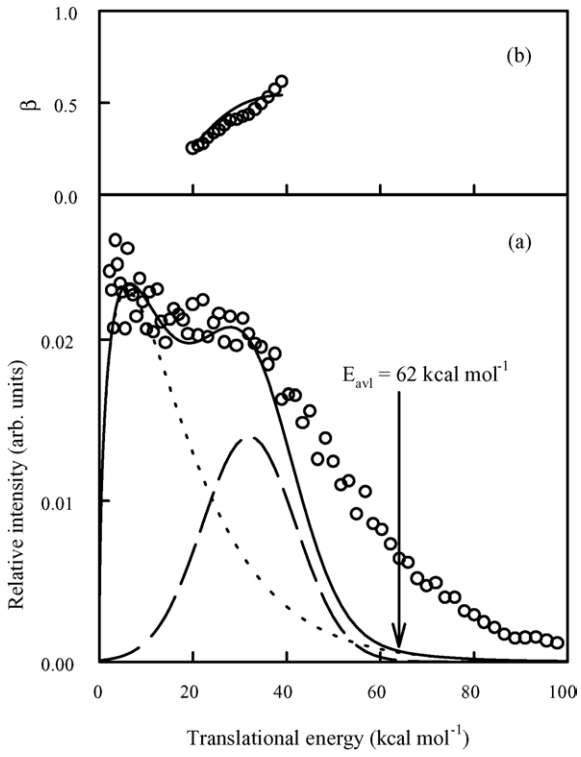

Fig. 6. Cl atom formation from $CDCl_3$ at 207 nm. (a) Center-of-mass translational energy distribution, $P(E_T)$. E_{avl} is the maximum available energy in the one-photon for reaction (5a). The broken and dotted curves are the best-fitted Gaussian and Maxwell–Boltzmann distributions, respectively. See Table 3 for the fitting parameters. The solid curve is a sum of the two distributions. The unresolved area is a contribution of two-photon process. (b) Angular anisotropy parameters. The solid curve is the best-fit distribution obtained by Eq. (11) with $a = 0.4$.

4.2. Photodissociation of $CDCl_3$ at 205–207 nm

4.2.1. Formation of Cl atom

The C_{3v} symmetry of $CDCl_3$ demands that transitions be polarized along the three-fold axis ($A_1 \leftarrow A_1$) or in the plane perpendicular to the three-fold axis ($E \leftarrow A_1$). If ψ is the D–C–Cl bond angle and the direction of dissociation is assumed to be a C–Cl bond, then, for a $A_1 \leftarrow A_1$ transition and prompt dissociation, $\beta = 2P_2(\cos\psi)$. For a $E \leftarrow A_1$ transition, $\beta = 2P_2(\cos(\pi/2))P_2(\cos\psi)$. The calculated β values with $\psi = 108^\circ$ are -0.71 for the $A_1 \leftarrow A_1$ transition, and 0.36 for the $E \leftarrow A_1$ transition [11]. Since the present β value for Cl is 0.7 ± 0.2, the formation of Cl is attributed to the $E \leftarrow A_1$ transition.

Yang et al. [11] reported the photodissociation of $CHCl_3$ at 193 nm by photofragment translational spectroscopy, in which only one fast component of chlorine fragments with $\beta = 0$ was observed. These results are in disagreement with ours. The reason for this disagreement is not clear.

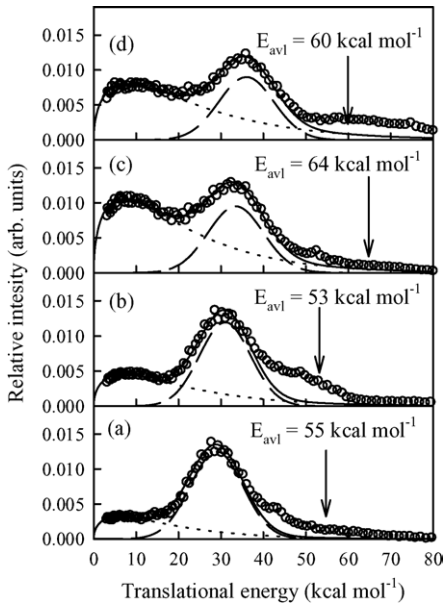

Fig. 7. Center-of-mass translational energy distributions for (a) Cl, (b) Cl^* from CF_2Cl_2, and (c) Cl, (d) Cl^* from $CFCl_3$ at 207nm (Cl) and 209 nm (Cl^*). E_{avl} denotes the maximum available energies for one-photon dissociation of reactions (6a)–(7b). The broken and dotted curves are the best-fitted Gaussian and Maxwell–Boltzmann distributions, respectively. See Table 3 for the fitting parameters. The solid curve is a sum of the two distributions.

4.2.2. Formation of D atoms

Based on the present results, the direct C–D rupture from cold $CDCl_3$ in a molecular beam is characterized by $\beta = 2.2 \pm 0.3$ and is assigned mainly to the $A_1 \leftarrow A_1$ transition, in which the dipole direction is parallel to the C-D axis and the maximum β value is 2. The present experiment shows that 90% of D atoms are formed from the indirect C–D bond rupture via a one-photon process. Brownsword et al. [13] reported the H atom formation from the photodissociation of $CHCl_3$ at 193 nm under room temperature condition. In their experiment, the H atom is produced from the secondary photodissociation of the $CHCl_2$ radical. The secondary photodissociation processes are likely enhanced because of the adequate internal energy of the primary photofragment, $CHCl_2$, under room temperature conditions, which may conceal the presence of the direct C–H rupture.

4.3. Photodissociation of CF_2Cl_2 and $CFCl_3$ at 207 and 209 nm

4.3.1. CF_2Cl_2

Since CF_2Cl_2 possesses C_{2v} symmetry, the maximum β_Y value for direct C–Cl rupture is calculated to be 1.09 for the *Y*-polarized transition that is perpendicular both to the C_2 axis and the F–C–F molecular plane, assuming that the Cl–C–Cl angle is 113° in the ground state CF_2Cl_2 [16]. The present β values of Cl and Cl^* from the direct rupture processes are 1.1 ± 0.1 and 1.4 ± 0.1, respectively, which are in good agreement with the theoretical limit. Therefore, the observed direct C–Cl rupture may be assigned to the $B_1 \leftarrow A_1$ transition.

Yen et al. [15] reported the energy distributions and β values of Cl and Cl^* from CF_2Cl_2 at 187 nm. They resolved the energy distribution into three components while we resolved into two components. Their product ratio of the highest energy component is 0.7 both for Cl and Cl^*, which is in agreement with our values, 0.8 ± 0.1 for Cl and 0.7 ± 0.1 for Cl^*. Their highest energy component is assigned to the direct C–Cl bond rupture with $\beta = 0.5$ and two lower energy ones with $\beta = 0.2$ and 0.1. However, their β value of 0.5 is not in agreement with our values of 1.1–1.4. The mixing of electronically excited potential energy surfaces might occur at the shorter wavelength due to vibrational mode excitation. Baum et al. [16] investigated the photodissociation process of CF_2Cl_2 at 193 nm by photofragment translational spectroscopy. They observed only one component of chlorine fragments with $\beta = 0.65$ and attributed the smaller β value to the rotation of the parent molecule. The reason for the lack of the slower energy component in their results is not clear.

4.3.2. $CFCl_3$

$CFCl_3$ possesses C_{3v} symmetry and the maximum β values are $-2/3$ for the $A_1 \leftarrow A_1$ transition and 1/3 for the $E \leftarrow A_1$ transition, assuming the tetrahedral structure in the ground state of $CFCl_3$. Since the present β values for Cl and Cl^* are positive (0.3), the direct C–Cl rupture is attributed to the prompt dissociation via the $E \leftarrow A_1$ transition.

Both energy distributions of Cl and Cl^* photofragments from $CFCl_3$ at 187 nm reported by Yen et al. [15] consisted of three components: the highest energy component assigned to the direct C–Cl bond rupture with $\beta \sim 0.5$ and two lower energy ones with $\beta \sim 0.2$. Their product ratio of the highest energy component is 0.5 for Cl and 0.6 for Cl^*, which are in agreement with our value, 0.4 ± 0.1 for Cl and 0.5 ± 0.1 for Cl^*. Felder et al. [17] investigated the photodissociation process of $CFCl_3$ at 193 nm by photofragment translational spectroscopy. They observed only the fast component of chlorine fragments with $\beta = 0.74$, which is above the theoretical upper limit. They tentatively attributed this discrepancy to a Jahn–Teller type distortion of the electronically excited potential energy surface. The theoretical calculations of the potential energy surface of the $CFCl_3$ electronic states may give further information on this problem.

4.4. Direct and indirect dissociation channels

Recently, Takahashi and his coworkers [14] have found in their vacuum ultraviolet laser-induced fluorescence experiments of the photodissociation of CF_2Cl_2, $CFCl_3$, $CHFCl_2$, CH_2Cl_2 and $CHCl_3$ at 193 nm that (a) each translational energy distribution of the chlorine photofragments has the high and low energy components, and (b) the total quantum yield for Cl and Cl^* is unity. Their results suggest that the low energy component comes from the one-photon dissociation process of the parent molecule and not from the secondary dissociation of vibrationally excited radical fragments. Hence, it could be concluded that in the photoprepared parent molecules at around 200 nm the strong coupling of the Rydberg states with the vibrationally excited ground state causes the slow component of Cl and Cl^* through the indirect dissociation path [31].

The contribution of the direct dissociation process shows a characteristic difference between two-chlorinated and three-chlorinated molecules (Table 3). The *a* values of CH_3CFCl_2 and CF_2Cl_2 are 0.7–0.8, while those of $CDCl_3$ and $CFCl_3$ are 0.4–0.5. In the photodissociation at 187 nm, Yen et al. [15] reported that the product ratios of the highest translational energy components from CF_2Cl_2 are 0.7 and those from $CFCl_3$ are 0.5–0.6. These results indicate that the number of Cl atoms in the molecular structure influences the *a* values. Zou et al. [32] reported the complicated dissociation dynamics of the $CHBr_2$ radical compared with CH_2Br. Their Raman spectra are active not only in the C–Br stretch but in the Br–C–Br bending mode and combinations of these modes in $CHBr_2$, suggesting more multidimensional photodissociation pathways for $CHBr_2$ than for CH_2Br. From this it can be concluded that the contribution of the simple direct dissociation pathway decreases with increasing the number of the C–Cl bonds.

5. Conclusions

Formation of chlorine atoms and hydrogen atoms from the photodissociation of CH_3CFCl_2 and $CDCl_3$ has been studied with use of one-color photofragment imaging spectroscopy. The velocity distributions of Cl atoms from CH_3CFCl_2 at 207–209 nm consist of fast and slow components. The fast one comes from the direct C–Cl rupture and is characterized by the angular anisotropy parameter, $\beta = 0.6 \pm 0.1$, while the slow one comes from the indirect C–Cl rupture via the hot parent

molecule mechanism and is characterized by $\beta = 0$. The fast one accounts for 70% of the total Cl yield. The velocity distributions of hydrogen atoms also have two different components. The fast one is characterized by $\beta = -0.6 \pm 0.2$, accounting for 70% of the total hydrogen atom yield. From these results, the photoexcitation of CH_3CFCl_2 at 205–209 nm is inferred to proceed via a mixture of the $A' \leftarrow A'$ and $A'' \leftarrow A'$ transitions for direct cleavage of the C–Cl bond, while via the $A' \leftarrow A'$ transition for direct cleavage of the C–H bond. About the Cl atoms from $CDCl_3$, the fast component is characterized by $\beta = 0.7 \pm 0.2$, accounting for 40% of the total Cl yield. The angular distribution of the fast D atom is characterized by $\beta = 2.2 \pm 0.3$, accounting for 10% of the total D yield. From these results, the photoexcitation of $CDCl_3$ at 205–207 nm is inferred to proceed mainly via the $E \leftarrow A_1$ transition for direct cleavage of the C–Cl bond, while via the $A_1 \leftarrow A_1$ transition for direct cleavage of the C–D bond.

References

[1] M.J. Molina, F.S. Rowland, Nature 249 (1974) 810.
[2] R.P. Wayne, Chemistry of Atmospheres, 2nd ed., Oxford University Press, New York, 1991.
[3] D.G. Ralph, R.P. Wayne, J. Photochem. 17 (1981) 405.
[4] A.C. Brown, C.E. Canosa-Mas, A.D. Parr, J.M.T. Pierce, R.P. Wayne, Nature 341 (1989) 635.
[5] A.C. Brown, C.E. Canosa-Mas, A.D. Parr, K. Rothwell, R.P. Wayne, Nature 347 (1990) 541.
[6] A. Lauter, D. Suresh, H.-R. Volpp, J. Chem. Phys. 118 (2003) 5821.
[7] A. Melchior, I. Bar, S. Rosenwaks, J. Chem. Phys. 107 (1997) 8476.
[8] T. Einfeld, C. Maul, K.-H. Gericke, R. Marom, S. Rosenwaks, I. Bar, J. Chem. Phys. 115 (2001) 6418.
[9] M.E. Jacox, D.E. Milligan, J. Chem. Phys. 54 (1971) 3935.
[10] Y. Matsumi, K. Tonokura, M. Kawasaki, G. Inoue, S. Satyapal, R. Bersohn, J. Chem. Phys. 94 (1991) 2669.
[11] X. Yang, P. Felder, J.R. Huber, Chem. Phys. 189 (1994) 127.
[12] R.A. Brownsword, M. Hillenkamp, T. Laurent, R.K. Vasta, H.-R. Volpp, J. Wolfrum, J. Chem. Phys. 106 (1997) 1359.
[13] R.A. Brownsword, M. Hillenkamp, T. Laurent, R.K. Vasta, H.-R. Volpp, J. Wolfrum, J. Phys. Chem. A 101 (1997) 5222.
[14] F. Taketani, K. Takahashi, Y. Matsumi, J. Phys. Chem. A 109 (2005) 2855.
[15] M. Yen, P.M. Johnson, M.G. White, J. Chem. Phys. 99 (1993) 126.
[16] G. Baum, J.R. Huber, Chem. Phys. Lett. 203 (1993) 261.
[17] P. Felder, C. Demuth, Chem. Phys. Lett. 208 (1993) 21.
[18] D.W. Chandler, P.L. Houston, J. Chem. Phys. 87 (1987) 1445.
[19] Y. Sato, Y. Matsumi, M. Kawasaki, K. Tsukiyama, R. Bersohn, J. Phys. Chem. 99 (1995) 16307.
[20] T.F. Budinger, G.T. Gullberg, IEEE Trans. Nucl. Sci. 21 (1974) 2.
[21] R.N. Zare, Mol. Photochem. 4 (1972) 1.
[22] R. Bersohn, S.H. Lin, Adv. Chem. Phys. 55 (1969) 1915.
[23] G.E. Bush, K.R. Wilson, J. Chem. Phys. 56 (1972) 3626.
[24] M.B. Robin, Can. J. Chem. 63 (1985) 2032.
[25] H.M. Lambert, P.J. Dagdigian, J. Chem. Phys. 109 (1998) 7810.
[26] H.M. Lambert, P.J. Dagdigian, Chem. Phys. Lett. 275 (1997) 499.
[27] M.D. Person, P.W. Kash, L.J. Butler, J. Chem. Phys. 94 (1991) 2557.
[28] H. Guo, K.Q. Lao, G.C. Schatz, A.D. Hammerich, J. Chem. Phys. 94 (1991) 6562.
[29] Y. Amatatsu, K. Morokuma, S. Yabushita, J. Chem. Phys. 94 (1991) 4858.
[30] M. Kawasaki, S.J. Lee, R. Bersohn, J. Chem. Phys. 63 (1975) 809.
[31] M.B. Robin, Higher Excited States of Polyatomic Molecules, vol. 1, Academic Press, New York, 1974.
[32] P. Zou, J. Shu, T.J. Sears, G.E. Hall, S.W. North, J. Phys. Chem. A 108 (2004) 148.